One-dimensional Ablation Analysis of Lightweight CFRP Ablators with Coking

By Sumio KATO,[1] Shoichi MATSUDA,[1] Naoyuki SHIMADA,[2] Shunsuke SAKAI,[1]
Keiichi OKUYAMA,[3] Bianca SZASZ,[4] and Takayuki SHIMODA[5]

[1]Department of Mechanical Systems Engineering, University of the Ryukyus, Nishihara-cho, Japan,

[2]Asahi Kinzoku Kogyo Inc., Anpachi-gun, Japan

[3]Department of Applied Science for Integrated System Engineering, Kyushu Institute of Technology, Kitakyushu, Japan

[4]Department of Mechanical System Engineering, Nagoya University, Nagoya, Japan

[5]Institute of Space and Astronautical Sicence, JAXA, Sagamihara, Japan

The coking phenomenon within a lightweight carbon-phenolic ablator exposed to the heating environment of air is investigated. The existing one-dimensional charring ablation analysis code is modified so that the coking behavior of the ablator can be calculated as well as the thermal response behavior within a lightweight carbon-phenolic ablator. The mass conservation equations for a pyrolysis gas and carbon in the gas are given. The energy equation including the coking process is also presented. The measured density distributions of some arc-heated CFRP ablator samples are compared with those calculated by the ablation analysis code, from which good agreement is obtained. The density profiles with and without coking are compared. The effect of temperature dependency of carbon mass fraction in a pyrolysis gas in the coking equation upon the density profile is examined. The effect of heating rate upon the density distribution in an ablator is also examined. The effect of coking upon the surface recession is studied analytically and experimentally.

Key Words: Ablation, Coking, Lightweight Ablator, Heat Shield, Re-Entry Capsule

Nomenclature

C_p : specific heat, J/(kg·K)

C_1, C_2 : tuning coefficients for thermal conductivity of virgin and char materials, respectively

h : enthalpy, J/kg

k : thermal conductivity, W/(m·K)

$\dot{m}_g$: mass flux of pyrolysis gas, kg/(m²·s)

q : heat flux, W/m² or MW/m²

q_{cw} : cold wall convective heat flux, W/m² or MW/m²

q_{net} : net heat flux, W/m²

S or ΔS : surface recession, m or mm

$\dot{S}$: surface recession rate, m/s

T, T_{ref} : temperature, K and 300K, respectively

t : time, s

x : moving coordinate or in-depth distance from receding surface, y - S, m or mm

y : stationary coordinate or in-depth distance from initial front surface, m or mm

Δh_{pyro} : heat of pyrolysis per gas produced, J/kg

ε : surface emissivity

ϕ_{blow} : blowing correction factor

ρ : density of ablator excluding ρ_{coke}, kg/m³

ρ_{coke} : density of deposited carbon due to coking, kg/m³

ρ_s : density at the surface, kg/m³

σ : Stefan-Boltzmann constant, 5.67×10^{-8} W/(m²·K⁴)

ω_c : carbon mass fraction of pyrolysis gas

ω_{c_cold} : ω_c for frozen pyrolysis gas (see Fig. 3)

ω_{c_pyro} : ω_c for pyrolysis gas during decomposition

ω_{c_upper} : ω_c for equilibrium pyrolysis gas (see Fig. 3)

Subscripts

ab, ch : ablation and char

coke, g : deposited carbon and pyrolysis gas

ref, u : reference and at wall underside

v, w : virgin material and at wall

1. Introduction

A re-entry capsule has the heat shield system to protect the inner equipment against severe heating conditions during re-entry. The heat shield system mainly consists of an ablator which has the capability to prevent heat transfer to the inside by ablation phenomena. Various kinds of ablative materials with various densities have been developed. [1-9] Among them, the carbon-phenolic ablator (CFRP ablator) has been applied to the earth re-entry capsules such as the USERS REV capsule (Unmanned Space Experiment Recovery System REcovery Vehicle) [6] and the re-entry capsule "Hayabusa", [8] and the planetary entry probe "Gallileo" of NASA. [5] Each of these capsules used a high density ablator with the value of about 1500 kg/m³. A lightweight CFRP ablator of about 300 kg/m³

has also been developed[4] and was used for the heat protection of the Stardust Capsule [7] of NASA.

Recently, a lightweight carbon-phenolic ablator named LATS (Lightweight Ablator series for Transfer vehicle Systems) with the density of 200 – 700 kg/m^3 has been developed. [9, 10] The LATS is a carbon-phenolic ablator (CFRP ablator) fabricated by impregnating a phenolic resin into a felt made of carbon fibers. The material properties of the LATS ablator were measured and arc-heated tests of the ablator samples with various densities were carried out. Measured in-depth temperatures were compared with the calculated results using a one-dimensional ablation analysis code. [9, 10]

The ablation phenomena of the CFRP material are very complicated, including the surface recession, radiation from the surface, generation of the pyrolysis gas from the resin, heat conduction within the ablator, the coking phenomenon, etc. The density changes due to the pyrolysis and coking, and the in-depth temperature decreases as the distance from the surface increases. The concept of charring ablation including coking is shown in Fig. 1, which is based on Refs. 11) and 12). The coking phenomenon is that a solid carbon is deposited when the pyrolysis gas passes through the porous char to the surface. The coking phenomenon increases the char density near the surface of the heated material, [12,13] which would influence the surface recession, mass, and heat resistance characteristics of the ablator. A charring ablator under heating is typically divided into three zones: char, pyrolysis, and virgin zones. The char zone includes the surface, the pyrolysis zone is next to the char zone, and the virgin zone is located deepest in the ablator. In the char zone, pyrolysis from the resin is almost finished. In the pyrolysis zone a certain amount of resin remains, from which the pyrolysis gas is generated. In the virgin zone, no pyrolysis gas is generated. If coking is not considered, the densities of the char, pyrolysis and virgin zones are the lowest, the second lowest and the highest, respectively. Coking occurs mainly in the char zone.

Until now, few researches [12,13] have been carried out concerning the coking behavior of the ablator. Among a lot of papers [10, 12 - 19] which treat ablation analysis in an ablator, only few treat coking analysis. [12,13] In Ref. 13), the coking behavior of the Apollo heat shield consisting of a low density ablation material was investigated analytically and experimentally, in which the material is Avcoat 5026-39/ HC-GP, a low-density
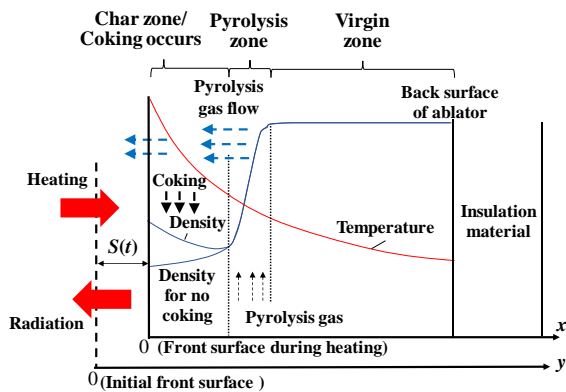
epoxy novolac resin with phenolic microballoons and silica fiber reinforcement in a fiberglass honeycomb matrix. In Ref. 12), the coking behavior of a low density CFRP ablator (the LATS ablator) in a N$_2$ environment, in which no surface recession is expected, was investigated analytically and experimentally.

In this paper, the coking phenomenon within a lightweight carbon-phenolic ablator (the LATS ablator) exposed to the aerodynamic heating environment of air with a surface recession is investigated. The existing one-dimensional charring ablation analysis code[10] is modified so that the coking behavior of the ablator can be calculated as well as the thermal response behavior within a lightweight carbon-phenolic ablator. The mass conservation equations for the pyrolysis gas and carbon in the gas are given. The energy equation including the coking process is also presented. The measured temperatures and density distributions of some arc-heated CFRP ablator samples are compared with the calculated results by using the ablation analysis code. The in-depth density profiles of an ablator heated in an arc-jet wind tunnel using air with and without coking are calculated and compared. The effect of temperature dependency of carbon mass fraction in the pyrolysis gas in the coking equation upon the density profile is examined. The effect of heating rate upon the density distribution in an ablator is also examined. The effect of coking upon the surface recession is studied analytically and experimentally.

2. Charring Ablation Analysis with Coking

A mathematical model for the analysis of one-dimensional charring ablation with coking and thermal response within an ablator[12,13] is described. The mass conservation equations with respect to the pyrolysis gas and the solid carbon, and the energy equation are explained. The boundary conditions and the material properties of the ablator are also described.
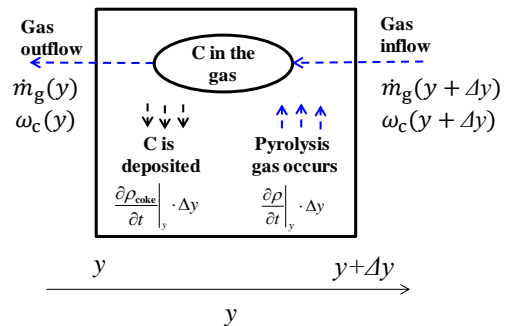
2.1. Mass balance for the pyrolysis gas

Fig. 2. Coking model in a control volume.

Consider a small control volume of the ablator, which is shown in Fig. 2. This figure is based on Ref. 12). It is assumed that the pyrolysis gas flows in and out of the volume along the y axis. It is also assumed that within the control volume, thermal decomposition yields the generation of the pyrolysis gas and solid carbon is deposited due to coking. Consideration of the mass balance with respect to the pyrolysis gas, in which

Fig. 1. Concept of charring ablation with coking.

the time derivative of the pyrolysis gas density is assumed to be small, gives the following equation

$$\Delta y \cdot \left.\frac{\partial \rho}{\partial t}\right|_y + \Delta y \cdot \left.\frac{\partial \rho_{\text{coke}}}{\partial t}\right|_y = \dot{m}_g(y + \Delta y) - \dot{m}_g(y) \tag{1}$$

where y is the stationary coordinate with the origin fixed to the initial ablator surface before heating (m), ρ is the density of the ablator without deposited carbon (kg/m³), ρ_{coke} is the density of the deposited carbon due to coking (kg/m³) (then, $\rho + \rho_{\text{coke}}$ is the density of the ablator), Δy is the width of the control volume (m), and $\dot{m}_g(y)$ is the mass flux of the pyrolysis gas which passes through the y-plane to the surface (kg/(m²·s)). Dividing both sides of Eq. (1) by Δy and $\Delta y \rightarrow 0$ yield

$$\left.\frac{\partial \rho}{\partial t}\right|_y + \left.\frac{\partial \rho_{\text{coke}}}{\partial t}\right|_y = \left.\frac{\partial \dot{m}_g}{\partial y}\right|_t \tag{2}$$

The terms on the left side of Eq. (2) represent time derivatives of ρ and ρ_{coke} respectively, and the term on the right side represents the gradient of mass flux of the gas with respect to y. The first term on the left side of Eq. (2) is given by the Arrhenius type expression for the decomposition rate and is described by

$$\left(\frac{\partial \rho}{\partial t}\right)_y = -\sum_{k=1}^{N} A_k f_k (\rho_v - \rho_{\text{ch}}) \left(\frac{\rho - \rho_{\text{ch}}}{\rho_v - \rho_{\text{ch}}}\right)^{\mu_k} \exp\left(-\frac{B_k}{T}\right) \tag{3}$$

where T is the temperature (K), μ_k is the reaction order, A_k is the weighting factor, f_k is the collision frequency (1/s), B_k is the activation temperature (K). The values of μ_k, A_k, f_k, and B_k are assumed to be constant. In Refs. 12) and 13), the term $\partial \rho / \partial t|_y$ on the left side of Eq. (2) is omitted because of its small value for coking calculation in the char layer. However the term $\partial \rho / \partial t|_y$ is not omitted in this paper.

2.2. Mass balance for carbon

When a solid carbon is deposited within a control volume of the ablator, the mass balance of carbon yields

$$\omega_c(y + \Delta y) \cdot \dot{m}_g(y + \Delta y) - \omega_c(y) \cdot \dot{m}_g(y)_y$$

$$= \Delta y \cdot \omega_{c\_pyro} \left.\frac{\partial \rho}{\partial t}\right|_y + \Delta y \cdot \left.\frac{\partial \rho_{\text{coke}}}{\partial t}\right|_y \tag{4}$$

where ω_c is the carbon mass fraction in a pyrolysis gas, and ω_{c_pyro} is the carbon mass fraction of the pyrolysis gas during thermal decomposition. We assume that ω_c is a function of the temperature.[12,13] In Ref. 13), the function ω_c was studied
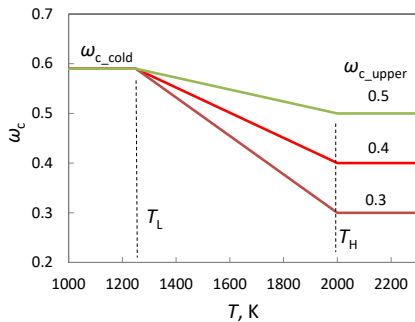

Fig. 3. Relation between ω_c and T.

for coking study. In Ref. 12) the function ω_c was used for coking calculation. In the present study we also use the

function ω_c shown in Fig. 3, which is based on that of Ref. 12).

When both sides of Eq. (4) are divided by Δy, and Δy decreases to zero, we obtain

$$\omega_c(y) \cdot \frac{\partial \dot{m}_g(y)}{\partial y} + \dot{m}_g(y) \cdot \frac{\partial \omega_c(y)}{\partial y} = \omega_{c\_pyro} \left.\frac{\partial \rho}{\partial t}\right|_y + \left.\frac{\partial \rho_{\text{coke}}}{\partial t}\right|_y \tag{5}$$

Eliminating $\partial \rho_{\text{coke}} / \partial t)_y$ from Eqs. (2) and (5) and substituting ω_{c_cold} for ω_{c_pyro} yields (In this paper, ω_{c_pyro} is assumed to be a constant value of ω_{c_cold}.)

$$\left.\frac{\partial \dot{m}_g}{\partial y}\right|_t = \frac{1 - \omega_{c\_cold}}{1 - \omega_c} \left.\frac{\partial \rho}{\partial t}\right|_y + \frac{\dot{m}_g}{1 - \omega_c} \left.\frac{\partial \omega_c}{\partial y}\right|_t \tag{6}$$

In a similar way, eliminating $\partial \dot{m}_g / \partial y)_t$ from Eqs. (2) and (5) and substituting ω_{c_cold} for ω_{c_pyro} yields

$$\left.\frac{\partial \rho_{\text{coke}}}{\partial t}\right|_y = \frac{\omega_c - \omega_{c\_cold}}{1 - \omega_c} \left.\frac{\partial \rho}{\partial t}\right|_y + \frac{\dot{m}_g}{1 - \omega_c} \left.\frac{\partial \omega_c}{\partial y}\right|_t \tag{7}$$

In Refs. 12) and 13), the first terms including $\partial \rho / \partial t|_y$ on the right side of Eqs. (6) and (7) are omitted for the coking calculation in the char layer because of the small values; in this paper, these terms are not omitted.

When the term on the left side of Eq. (7) is expressed on the moving axis of x, we obtain

$$\left.\frac{\partial \rho_{\text{coke}}}{\partial t}\right|_x = \frac{\omega_c - \omega_{c\_cold}}{1 - \omega_c} \left.\frac{\partial \rho}{\partial t}\right|_y + \frac{\dot{m}_g}{1 - \omega_c} \left.\frac{\partial \omega_c}{\partial y}\right|_t + \dot{S} \left.\frac{\partial \rho_{\text{coke}}}{\partial x}\right|_t \tag{8}$$

where x is the moving coordinate or in-depth distance from the receding surface (m), and $\dot{S}$ is the surface recession rate (m/s).

In Fig. 3 the pyrolysis gas is assumed to be frozen ($\omega_c = \omega_{c\_cold}$) below the temperature T_L and to be in equilibrium ($\omega_c = \omega_{c\_upper}$) above the temperature T_H. At intermediate temperatures, the amount of carbon ω_c is assumed to vary linearly from T_L to T_H. In the figure $T_L = 1250K$, $T_H = 2000K$, $\omega_{c\_cold} = 0.59$, $\omega_{c\_upper} = 0.3$, 0.4, and 0.5. During the heating of an ablator, the pyrolysis gas passes through the char layer to the surface (Fig. 1). When the temperature T is below T_L or above T_H, ω_c is constant, then from Eq. (7) $\partial \rho_{\text{coke}} / \partial t$ is depressed; coking is depressed. For T between T_L and T_H, if $\partial T / \partial x$ (= $\partial T / \partial y$) is negative (Fig. 1), $\partial \omega_c / \partial y = (\partial T / \partial y)(\partial \omega_c / \partial T)$ becomes positive and $\partial \rho_{\text{coke}} / \partial t$ increases; coking occurs (see Eq. (7)). When ω_{c_upper} decreases, the absolute value of $\partial \omega_c / \partial T$ increases, from which the amount of coking increases. This means that the lower value of ω_{c_upper} promotes coking. (Note: In this mathematical model for coking, if the sign of $\partial T / \partial x$ (= $\partial T / \partial y$) changes from negative to positive values, $\partial \omega_c / \partial y$ becomes negative and $\partial \rho_{\text{coke}} / \partial t$ decreases.)

2.3. Energy equation

The in-depth energy conservation equation of the ablator including coking process is basically the same as those of Refs. 12) and 13) and is given by

$$(\rho C_p + \rho_{\text{coke}} C_{\text{pcoke}}) \left.\frac{\partial T}{\partial t}\right|_x = \frac{\partial}{\partial x}\left(k \frac{\partial T}{\partial x}\right) + \Delta h_{\text{pyro}} \left.\frac{\partial \rho}{\partial t}\right|_x$$

$$+ \dot{m}_g C_{\text{pg}} \left.\frac{\partial T}{\partial x}\right|_t + (h_g - h_{\text{coke}}) \left.\frac{\partial \rho_{\text{coke}}}{\partial t}\right|_y + \dot{S}(\rho C_P + \rho_{\text{coke}} C_{\text{pcoke}}) \left.\frac{\partial T}{\partial x}\right| \tag{9}$$

where k is the thermal conductivity (W/(m·K)); C_p, C_{pcoke} and C_{pg} are the specific heats of the ablator without deposited carbon, deposited carbon due to coking, and the pyrolysis gas, respectively (J/(kg·K)); h_{coke} and h_g are the enthalpies of deposited carbon due to coking and the pyrolysis gas (J/kg), respectively; Δh_{pyro} is the heat of pyrolysis per gas produced (J/kg). The terms in Eq. (9) represent, from left to right, the sensible energy accumulation, the net conduction, the energy absorbed during pyrolysis, net energy convected by the pyrolysis gas passing through, the energy due to the deposition of carbon by coking, net energy convected as the consequence of coordinate motion.

The thermal conductivity k is calculated by

$$(\rho + \rho_{coke})k = \omega_1 \rho_v k_v + (1 - \omega_1)\rho_{ch} k_{ch} \tag{10a}$$

$$\omega_1 = (\rho + \rho_{coke} - \rho_{ch})/(\rho_v - \rho_{ch}) \tag{10b}$$

where subscripts of v and ch represent virgin and char, respectively. In the case of no coking ($\rho_{coke} = 0$), Eq. (10)a and (10)b have been used for ablation analysis.[10, 15-16] In this paper we assume that Eqs. 10)a and 10)b can also be used for the case of coking ($\rho_{coke} \neq 0$). Considering that the thermal conductivity is tuned based on the matching of measured and calculated results (see Subsection 2.5.), and the measured and calculated temperatures agree well (see Section 4.), the approximation of k by Eqs. (10a) and (10b) seems not to have large errors. (This assumption of thermal conductivity would cause a certain amount of errors; in the future it would be desirable to improve the thermal conductivity based on the measured data of char material including the coked material.)

The volumetric heat capacity of the char material including the coked material is expressed by the sum of ρC_p and $\rho_{coke} C_{pcoke}$, where ρC_p (volumetric heat capacity of the char excluding the coked material) is expressed[10, 14] by Eqs. (10c) and (10d), and $\rho_{coke} C_{pcoke}$ (volumetric heat capacity of the coked material) is expressed by the product of ρ_{coke} and C_{pcoke} of Eq. (15).

$$\rho C_p = \omega_2 \rho_v C_{pv} + (1 - \omega_2)\rho_{ch} C_{pch} \tag{10c}$$

$$\omega_2 = (\rho - \rho_{ch})/(\rho_v - \rho_{ch}) \tag{10d}$$

2.4. Boundary conditions

The energy balance at the ablator surface yields the surface boundary condition, in which aerodynamic heating, block effect of heating due to the mass ejection, radiation cooling, and enthalpy change when the char recedes, enthalpy change of the pyrolysis gas and the heat conduction in the ablator are considered. We also assume that the pyrolysis gas is chemically inert with respect to the boundary layer gases.[15] Thus the surface boundary condition is obtained and is shown below [15]

$$q_{net} = q_{cw}(1 - h_w/h_r)\phi_{blow} - \varepsilon\sigma(T_w^4 - T_{ref}^4) - \dot{m}_{ab}(h_w - h_u) \tag{11}$$

where h_w is the enthalpy of the gas adjacent to the surface, h_r is the recovery enthalpy of the flow, T_w is the temperature of the char surface, T_{ref} is 300 K, $\dot{m}_{ab}(= (\rho_{ch} + \rho_{coke})\dot{S})$ is the mass flux due to the thermochemical ablation of the char, and h_u is the enthalpy of the char at the surface. ϕ_{blow} is the

blowing correction factor, which means the ratio of heat transfer coefficient with and without ablation mass injection into the boundary layer from the ablator surface. The factor ϕ_{blow} also means the correction (reduction) factor of heat flux due to the mass injection into the boundary layer.[15, 16]

As for the back surface boundary condition, the back surface of the ablator is attached to an insulation material, and the back surface of the insulation material is assumed to be at a constant value of 300 K.

2.5. Input data for material properties

Input data for calculating the thermal behavior of the ablator model using the program of one-dimensional ablation analysis with coking include parameters such as heating conditions, the material properties and ablator thickness. As for the input data of the ablator material properties, these are the same as those in the previous paper,[10] except for the material properties related to the deposited carbon due to coking. These are determined based on the measured and literature data. [4, 9, 10, 15-17]

The virgin density ρ_v of the ablator is set based on the measurement. The char density for each ablator model is calculated by means of the following relation based on the measurement of virgin and charred materials. [9]

$$\rho_{ch} = \rho_v \times 0.716 \tag{12}$$

The emissivity of the char surface is set to be 0.85.[10]

The reference value of thermal conductivity of the virgin material k_{v_ref} is constructed based on the measured values of the LATS materials with the density of about 300 kg/m³, combined with the literature data.[4] The reference value of thermal conductivity of the char material k_{ch_ref} is assumed to be the same as that of the virgin material k_{v_ref} ($k_{ch\_ref} = k_{v\_ref}$). Thermal conductivities of the ablator materials are expressed by $C_1 k_{v\_ref}$ and $C_2 k_{ch\_ref}$, where C_1 and C_2 are constant. The values of C_1 and C_2 are determined based on the matching of the measured and calculated temperatures,[10] in which the measured temperatures are obtained in the arc-heated tests of the ablators. (The details of the determination of C_1 and C_2 are described in Ref. 10).)

The specific heat of the char material C_{pch} (full char) is based on the following expression [15]

$$C_{pch} = C_\infty \frac{T}{\sqrt{T^2 + D^2}} \tag{13}$$

where T is the temperature (K), $C_\infty = 2.3 \times 10^3$ J/(kg·K), and $D = 800$ K. The specific heat of the virgin material C_{pv} is constructed of the measured data with the temperature range of RT(room tempertature) to 300 °C (573 K), combined with Eq. (13), in which the connection is made smoothly.

The enthalpy and the specific heat of the deposited carbon h_{coke} and C_{pcoke} are calculated by the following equations, respectively: [15]

$$h_{coke} = \int_{T_{ref}}^{T} C_p dT = C_\infty \left(\sqrt{T^2 + D^2} - \sqrt{T_{ref}^2 + D^2}\right) \tag{14}$$

$$C_{pcoke} = C_\infty \frac{T}{\sqrt{T^2 + D^2}} \tag{15}$$

where $T_{ref} = 300$ K, $C_\infty = 2.3 \times 10^3$ J/(kg·K) and $D = 800$ K. The enthalpy of the pyrolysis gas h_g is given by

$$h_g = h_f + \int_{T_0}^{T} C_{pg} dT = h_f + C_{pg}(T - T_0) \qquad (16)$$

where h_f is the standard heat of formation (= − 9.28 × 10⁶ J/kg)[20] and T_0 is the standard ambient temperature (= 298 K). The specific heat of the pyrolysis gas C_{pg} is set to be a constant value of 1674.6 J/(kg·K).[16] The heat of pyrolysis per gas produced Δh_{pyro} is set to be 3.313 × 10⁵ J/kg (79.1 cal/g), which is determined considering the measured and the literature data. Coefficients in the Arrhenius equation (Eq. (3)) are set based on the TGA data of the LATS ablator.[17] Values of $N = 2$, $A_1 = 0.1$, $f_1 = 3.5 × 10^9$ 1/s, $B_1 = 1.1 × 10^4$ K, $\mu_1 = 100.0$, $A_2 = 0.9$, $f_2 = 7.0 × 10^3$ 1/s, $B_2 = 1.1 × 10^4$ K, and $\mu_2 = 3$ are used in the calculation.

2.6. Calculation procedure

The temperature and the density distributions in the ablator and insulation material are calculated by the use of the equations mentioned above. Calculation is carried out using the finite difference method considering the boundary conditions. For each time step, ρ is calculated by Eq. (3). Equations (6) and (8) give $\dot{m}_g$ and ρ_{coke}, respectively with the assumption that the pyrolysis gas flow is zero at the back surface of the ablator. T is calculated by Eq. (9), in which the calculation results of ρ, ρ_{coke} and $\dot{m}_g$ are used. In the calculation ρ, $\dot{m}_g$, and T are obtained explicitly; ρ_{coke} is obtained implicitly.

The front surface condition of Eq. (11) and the back surface condition (attached to the insulation material) are also considered. In the calculation, $\dot{m}_{ab}$ is obtained considering oxidation (reaction controlled or diffusion controlled oxidation) and sublimation of the surface char.[15, 16] $\dot{S}$ is obtained by the relation of $\dot{S} = \dot{m}_{ab}/(\rho_{ch} + \rho_{coke})$. For each time step, output parameters are obtained simultaneously for both the ablator and the insulation material.

3. Arc-heated Tests

The objectives of the arc-heated tests are: (1) to observe the coking effect (tendency of the in-depth density distribution) in the LATS ablator, and (2) to compare the measured ablator density distribution with the calculated result, from which the validity of the mathematical model for coking is evaluated.

3.1. Heating tests

Arc-heated tests of several LATS ablator samples were carried out in two arcjet wind tunnels: a 20 kW arcjet wind tunnel at Japan Ultra-high Temperature Materials Research Center (JUTEM), and a 1 MW segmented type arcjet wind tunnel at the Institute of Space and Astronautical Science (ISAS) of the Japan Aerospace Exploration Agency (JAXA).

For testing in the 20 kW arcjet wind tunnel at JUTEM, air was used as a test gas. The cold wall heat flux rate, the impact pressure and the air enthalpy are 1.65 MW/m², 0.85 kPa and 23.0 MJ/kg, respectively. The heating time is 60 s. The density and sizes of each ablator sample are 323.4 kg/m³ and about 30 mmφ × 40 mm, respectively. To obtain the one-dimensional heating environment, the side of the ablator sample was covered with an insulation material which is supported by a Bakelite holder to protect against side heating. The ablator back surface is attached to an insulation material. Several thermocouples are placed within the ablator in the direction parallel to the front surface of the ablator near the center axis to measure the in-depth temperatures.

As for the test in the 1 MW arcjet wind tunnel at JAXA, air was used as a test gas in the same way as at JUTEM. The cold wall heat flux, the air enthalpy and the impact pressure are 1.85 MW/m², 9.3 kPa and 14.5 MJ/kg, respectively. The heating time is 30 s. The density and the sizes of the ablator sample are 598.6 kg/m³ and about 30 mmφ × 40 mm, respectively. To obtain a one-dimensional heating environment, the side of the ablator sample was covered with an insulation material which is supported by a Bakelite holder to protect against side heating. The back surface of the ablator is attached to the Bakelite holder. For the temperature measurement several thermocouples are placed within the ablator in the direction parallel to the front surface of the ablator near the center axis. The surface temperature of the ablator was measured by a pyrometer.

3.2. Measurement of density distribution of ablator

The procedure for the measurement is as follows:
(1) Each of the heated ablator samples is cut into several specimens parallel to the central axis by a micro-cutter, each of which has the cross section of a circular sector with the central angle of 90 or 180 degrees (JUTEM ablator: 90 deg., JAXA ablator: 180deg.) (2) Taking photographs of cross sections perpendicular to the axis (photograph S_1), and parallel to the axis (photograph S_2): S_1 is used for calculation of the cross-sectional area in (4), and S_2 is used for estimating the density distribution. (3) The specimen is shaved by a milling machine with a pitch of $\Delta L = 0.2$ mm (JAXA ablator) and 0.25 mm (JUTEM ablator). (4) After each shaving, the mass m_i and thickness L_i (L_i: average based on 5 places) of the remaining ablator are measured by using an electric balance and a pair of calipers, from which the density of each shaved section (slice) is calculated by using the value of the cross-sectional area S_1.

The density variations of the slices were very large. However, it was found that the density varies cyclically with a pitch of around 2 mm (JAXA ablator) or 3 mm (JUTEM ablator), and the shape of the curve was roughly similar for each cycle. Two kinds of one cycle intervals are used for averaging calculation: M-M interval (one cycle from the maximum point to the next maximum point) and V-V interval (one-cycle from the minimum point to the next minimum point). When the curve is approximated by $\rho = a\sin\theta + b$ (a and b: constant, θ: the phase angle), M-M interval corresponds to $\theta = $ --- $-3\pi/2$- $\pi/2$, $\pi/2$- $5\pi/2$, --- and V-V interval corresponds to $\theta = $ --- $-\pi/2$- $3\pi/2$, $3\pi/2$- $7\pi/2$, --- . It was found that based on the black-and-white gradient image data in the photograph of the section, maximum and minimum density points can be roughly estimated. In determining each interval (M-M, V-V) for average calculation, we not only use the density curve of the slices, but also use the photograph data of the section.

4. Results and Discussion

4.1. Comparison of calculated and measured results

4.1.1. Heating test at JUTEM

Figure 4 shows the in-depth temperature time histories at various locations of the ablator sample measured by using thermocouples during the arc-heated test at JUTEM. The cold wall heat flux rate is 1.65 MW/m² with the heating time of 60 s. The density of the sample is 323.4 kg/m³. The thermocouples are located at various distances from the surface near the center axis of the ablator. The temperature measured by the thermocouple of T_1 ($y = 5.0$ mm) rises very rapidly to the peak value of about 1500 K, where y is the location of the thermocouple from the initial front surface before heating. After the time of the peak, it decreases rapidly and monotonously, due to the termination of heating after 60 s from the beginning of the heating. In the similar way, the temperature of T_2 ($y = 10.7$ mm) rises to the peak value of about 800 K, in which the rising rate of T_2 is lower than that of T_1. After reaching the peak value, T_2 decreases monotonically. T_3 ($y = 20.8$ mm) increases very slowly, and after about 300 s decreases gradually. The temperature of T_4 ($y = 29.8$ mm) increases very slowly, and maintains a nearly constant value for about 500 – 600 s. As y increases, the rising rate of the temperature decreases, the peak temperature decreases, and the time for the peak temperature is delayed. The calculated temperatures at the corresponding four points are also shown in the figure for the purpose of comparison in which $C_1 = 0.95$, $C_2 = 1.05$, $\omega_{c\_cold} = 0.59$, and $\omega_{c\_upper} = 0.3$. It is seen that the measured and calculated temperatures at the four points agree well with each other. This means that the calculated temperatures in the ablator, upon which the accuracy of coking calculation is dependent, are considerably accurate.

Figure 5 shows the measured density of the ablator sample with respect to the x axis (x: distance from the surface after heating) in the region near the surface. It is seen that from $x \approx 2$ to $x \approx 4$ mm the density decreases as x increases. At $x \approx 4$ mm, the density is seen to have a minimum value of about 250 kg/m³, and for $x >$ about 6 mm the density increases as x increases. In the figure the calculated density distributions with coking $\rho + \rho_{coke}$ evaluated at $t = 600$ s are also shown for comparison, in which $C_1 = 0.95$, $C_2 = 1.05$, $\omega_{c\_cold} = 0.59$, and $\omega_{c\_upper} = 0.3$, 0.4 and 0.5. The calculated density distribution with $\omega_{c\_upper} = 0.3$ agrees well with that of measurement. From the figure it is seen that a lower value of ω_{c_upper} promote coking. The tendency of the density distribution for both measurement and calculation is that as x increases from the point near the surface, the density decreases, and after reaching the minimum value it increases. This tendency of the density profile is similar to that of the measured and calculated Apollo ablator.[13] The calculated density distribution without coking is also shown in Fig. 5. It is seen that the density calculated with no coking increases monotonously as x increases, and is lower than that calculated with coking in the region of x from 0 to about 4.5 mm, where the difference corresponds to the deposited carbon due to the coking effect. For x more than about 4.5 mm, the densities
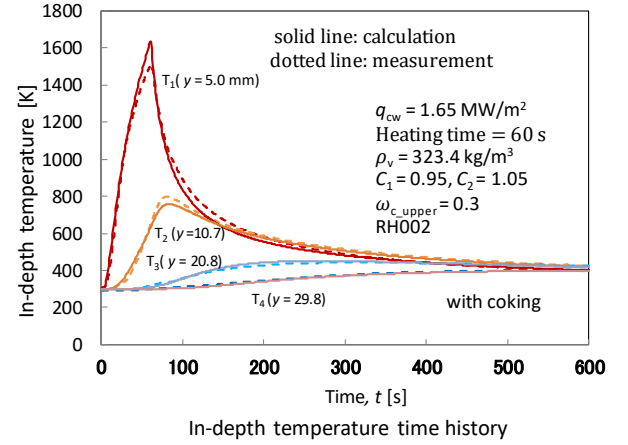

Fig. 4. Comparison of temperature time histories between measurement and calculation.
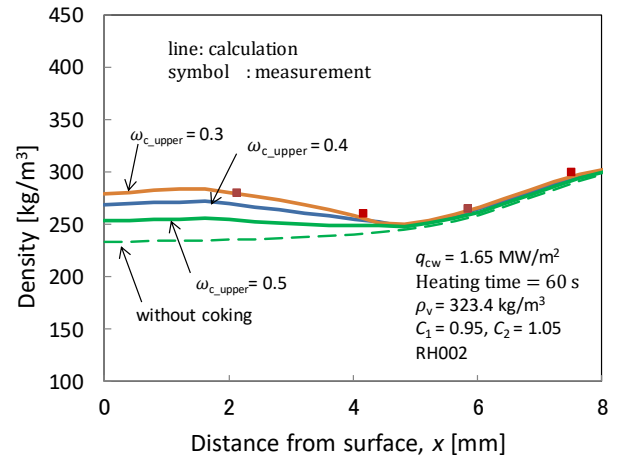

Fig. 5. Comparison of density distributions of arc-heated ablator between measurement and calculation.
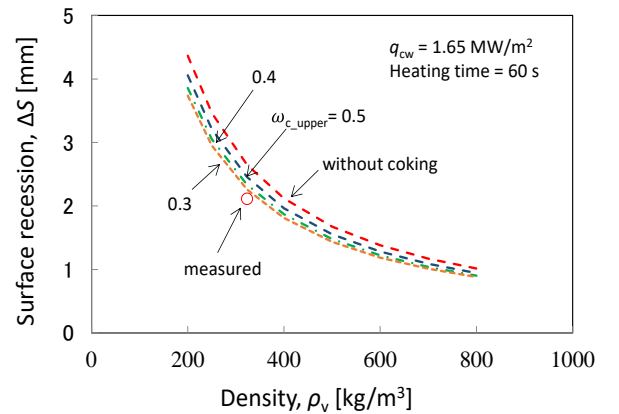

Fig. 6. Surface recession of ablator (results of calculation and measurement).

with and without coking are nearly the same. The calculated surface temperature is around 2250K, which suggests that the surface is in the diffusion controlled oxidation region.[15] In the case of diffusion controlled oxidation region, when we assume that the material is carbon and the heating environment is the same, the mass flux of oxygen $\dot{m}(O_2)$ is the same [21]; the surface mass loss $\dot{m}_{ab}$ ($= \rho_s \times \dot{S}$) is also the same. As the

surface density ρ_s increases, the surface recession rate $\dot{S}$ and also the surface recession ΔS decrease. Figure 6 shows the relation between the surface recession ΔS and the ablator density ρ_v calculated with the parameters of "without coking", ω_{c_upper} = 0.3, 0.4 and 0.5. The heating conditions for the calculation are the same as those of Figs. 4 and 5. The figure shows that ΔS decreases as ρ_v increases for each parameter.
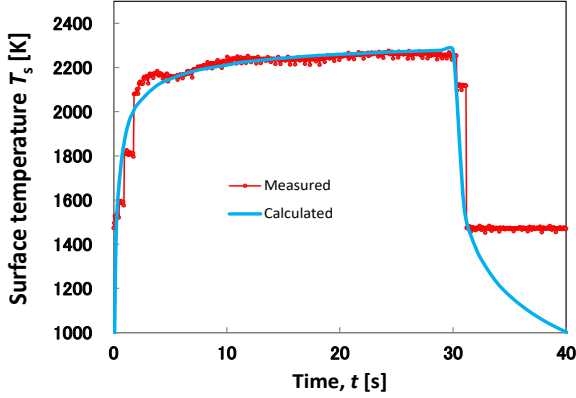

Fig. 7.   Comparison of surface temperature time histories between measurement and calculation.
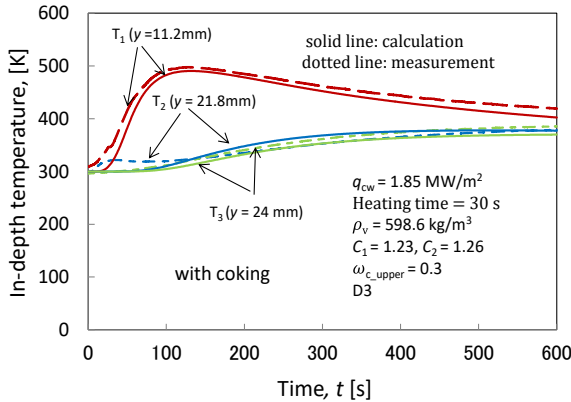

Fig. 8.   Comparison of in-depth temperature time histories between measurement and calculation.
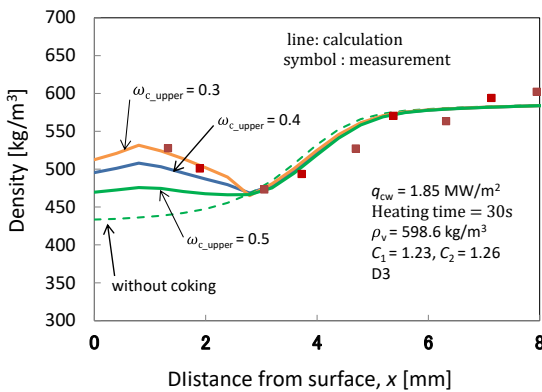

Fig. 9.   Comparison of density distributions of arc-heated ablator between measurement and calculation.

When ρ_v is higher, ρ_s is also higher, which gives the lower surface recession. It is seen that for a constant density of ρ_v, ΔS is the maximum for "without coking", the second maximum for ω_{c_upper} = 0.5, the third maximum for ω_{c_upper} =

0.4, and the minimum for ω_{c_upper} = 0.3. As seen from Fig. 5, ρ_s is the maximum for ω_{c_upper} = 0.3, the second maximum for ω_{c_upper} = 0.4, the third maximum for ω_{c_upper} = 0.5, and the minimum for "without coking". This and the relation of ρ_s and ΔS in the diffusion controlled oxidation region explain the tendency of ΔS for a constant ρ_v. A smaller value of ω_{c_upper} promote coking; the surface density increases, which decreases ΔS. The only one measured value of ΔS, which was obtained using the calipers, is also shown in Fig. 6. The measured ΔS is seen to be lower than those of four kinds of calculated values, in which the measured value is 80% and 93% of that for "without coking" and ω_{c_upper} = 0.3, respectively.

4.1.2.   Heating test at JAXA

Figure 7 shows the measured surface temperature T_s of the LATS ablator in the arc-heated test at JAXA, where the cold wall heating rate is 1.85 MW/m², the heating time is 30 s and the ablator density is 598.6 kg/m³. The surface temperature was measured by a pyrometer. At the beginning of the heating, T_s rises to the value of about 2200 K in about 2 - 3 s, and keeps nearly constant between 2200 and 2300 K before the heating is cut at the time of 30 s. The calculated temperature is also shown in the figure, where the measured and calculated temperatures agree fairly well. (The calculation conditions are the same for Figs. 7 – 9 except that ω_{c_upper} is 0.3 for Figs. 7 and 8, and the values of ω_{c_upper} are 0.3, 0.4 and 0.5 for Fig. 9.)

The measured in-depth temperature time histories by the thermocouples of T_1, T_2 and T_3 are shown in Fig. 8. The thermocouples are located at various distances from the surface near the center axis of the ablator. The temperature of T_1 (y = 11.2 mm) rises to the peak value of about 500 K. After the time of the peak, it decreases gradually monotonically, due to the cut of heating after 30 s from the beginning of the heating. In the similar way, the temperatures of T_2 (y = 21.8 mm), and T_3 (y = 24.0 mm) increase very slowly. At t = 600 s, T_2 and T_3 are still increasing. The calculated temperatures for T_1, T_2 and T_3 are also shown in the figure. It is seen that the measured and calculated temperatures agree well. This means that the calculated temperatures in the ablator, upon which the accuracy of coking calculation is dependent, are considerably accurate. It is seen that the rising behavior of the measured T_1 and T_2 do not agree with those of calculated temperatures, respectively. There is a possibility that during heating the high temperature air leaked through the gap between the support structure and the ablator in the front area and passed along the side of the ablator heating the thermocouple of T_1 and T_2.

Figure 9 shows the measured density of the ablator in the region near the surface. It is seen that from $x \approx$ 1.3 to $x \approx$ 3 mm the density decreases as x increases. At $x \approx$ 3 mm, the density is seen to have a minimum value of about 470 kg/m³, and for $x >$ about 3 mm the density increases as x increases. In the figure the calculated density distributions with coking evaluated at 600 s are also shown for comparison, where C_1 = 1.23, C_2 = 1.26, ω_{c_cold} = 0.59, and ω_{c_upper} = 0.3, 0.4 and 0.5. Agreement of the densities between measurement and calculation with coking is good for ω_{c_upper} = 0.3. The tendency of the density distribution for both measurement and

calculation is that as x increases from the point near the surface, the density decreases, and after reaching the minimum value it increases. This density tendency is the same as that in Fig. 5 and is similar to that of the measured and calculated Apollo ablator.[13] The calculated density distribution without coking is also shown in Fig. 9. It is seen that the density calculated without coking increases monotonously as x increases, and is lower than that calculated with coking in the region of x from 0 to about 3 mm, where the difference corresponds to the deposited carbon due to the coking effect. For x more than about 3 mm, the densities with and without coking are about the same.

In Fig. 9, in the region for $x <$ about 1mm, the density decreases as x decreases. Based on the results of coking calculation, the reason is estimated to be due to the following:

(1) During heating, a part of this region is higher than 2000K, where the coking is depressed.

(2) After the end of heating, pyrolysis gases pass through the char for certain time duration. For several seconds after the end of heating, the surface temperature decreases rapidly, which changes $\partial T/\partial x$ from negative to positive values. Then the mathematical model of coking decreases the density of the region near the surface during the short period after the end of heating.

With respect to (1) and (2), refer to the discussion of the mathematical model for coking in Subsection 2.2. The same behavior is also seen in Fig. 5. The validity of this behavior obtained by the mathematical model for coking in this paper should be examined experimentally in the future.

Figure 10 shows the distributions of ρ, ρ_{coke}, $\rho + \rho_{coke}$, at the time of 20 s after the beginning of the heating with ω_{c_upper} = 0.3. It is seen that coking occurs in the region from $x = 0$ to $x =$ about 2 mm. It is also seen that $\rho - \rho_{char}$ is not small and then $\partial \rho/\partial t$ is not small in this region, which means that omission of the first terms of the right hand side of Eqs. (6) - (7) would lead to a certain amount of errors. (In this paper we do not omit these terms; see Subsection 2.2.)

Figure 11 shows the relation between the surface recession ΔS and the ablator density ρ_v calculated with the parameters of "without coking", ω_{c_upper} = 0.3, 0.4 and 0.5. The heating conditions for the calculation are the same as those of Figs. 7 – 9. The only one measured value of ΔS is also shown in the figure. The tendency of the figure is the same as that of Fig. 6.
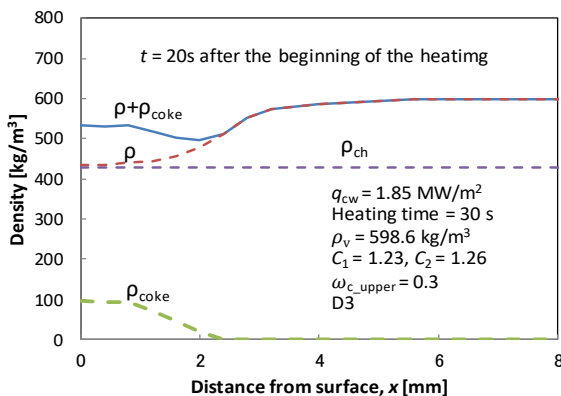

Fig. 10.   Density distribution during heating ($t = 20$s).

The measured ΔS, which was obtained using the calipers, is seen to be lower than those of four kinds of calculated values, in which the measured value is 55% and 67% of that for "without coking" and ω_{c_upper} = 0.3, respectively.
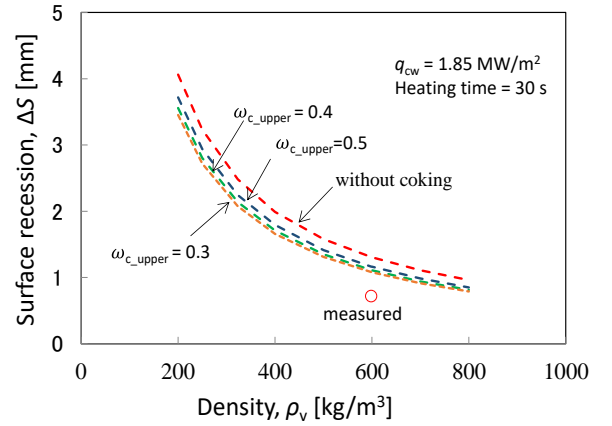

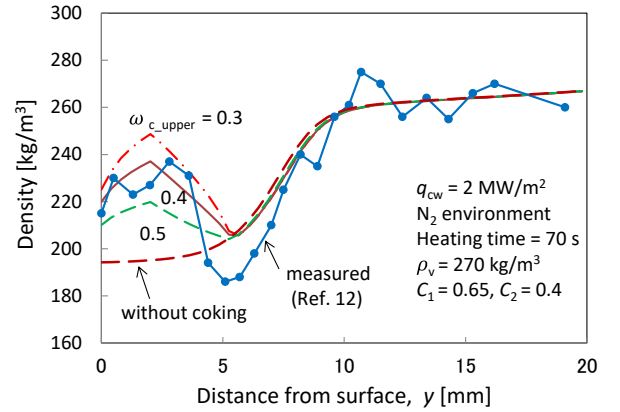Fig. 11.   Surface recession of ablator (results of calculation and measurement).

Fig. 12.   Comparison of the density distributions of ablator between measurement [12] and calculation.

4.2.   Comparison with the literature data

In Ref. 12), the measured densities of a low-density LATS ablator heated in the 20 kW arc-jet wind tunnel at JUTEM, in which Nitrogen was used as a test gas, were compared with the calculated results. The cold wall heat transfer rate, the impact pressure and the enthalpy were 2 MW/m², 0.8 kPa, and 9.2 MJ/kg, respectively. The heating time was 70 s. As Nitrogen was used, no surface recession was expected. Agreement between the measured and calculated results was satisfactory.

In order to confirm the validity of our ablation analysis code accounting for coking, ablation analysis of the same ablator under the same heating conditions is carried out by using our ablation analysis code, and the calculated results are compared with those of measurement. In Fig. 12 measured densities of the ablator[12] are compared with the ablator density distributions calculated by our ablation analysis code with the conditions of ω_{c_cold} = 0.59, and ω_{c_upper} = 0.3, 0.4, and 0.5. The calculated density with no coking is also included in the figure. The calculated densities are evaluated at $t = 600$ s. Agreement of the density distributions is seen to

be good especially for $\omega_{c\_upper} = 0.4$. The same result was also obtained in Ref. 12). This supports the validity of our ablation analysis code in which coking is included. The tendency of the density profile is similar to that in 4.1.1 and 4.1.2. The reasons for the coking behavior are the same as those described in 4.1.2. with respect to Fig. 9. In addition, the reason for the large density gradient near the surface is that the ablator has no surface recession.

4.3. Parametric study by ablation analysis

In order to understand the coking behavior in an ablator under heating, effects of some parameters upon the coking behavior are examined by coking analysis. Figure 13 shows the effect of ω_{c_upper} upon the density distributions $\rho + \rho_{coke}$ of a lightweight ablator with respect to the y axis with $q_{cw} = 1.65$ MW/m^2, $\rho_v = 323.4$ kg/m^3, and $\omega_{c\_upper} = 0.3$, 0.4 and 0.5. The density profile without coking and ρ for $\omega_{c\_upper} = 0.4$ are also included in the figure. The heating rate, the ablator length, etc. for the calculation are the same as those in Fig. 5. The calculated densities are evaluated at $t = 600$ s. The tip of each curve corresponds to the ablator surface. It is seen that the surface recession is roughly the same for each case. (Strictly, the surface recessions for $\omega_{c\_upper} = 0.3$, 0.4 and 0.5 are the smallest, the second smallest and the third smallest, respectively. The surface recession for no coking is the largest. The reason for this is that the higher the surface density is, the smaller the surface recession becomes; refer to the discussion of surface recession ΔS concerning Fig. 6 in 4.1.1 and Fig. 11 in 4.1.2.) As for each curve of the density $\rho + \rho_{coke}$ for three kinds of ω_{c_upper}, as y increases, the density increases from the surface to the maximum point at $y \approx 3.5$ mm, decreases to the minimum point at $y \approx 7$ mm, and then increases monotonously. It is seen that the coking process occurs in the region between the surface and $y \approx 7$ mm. The value of $\omega_{c\_upper} = 0.3$ in the coking region gives the maximum value of $\rho + \rho_{coke}$, $\omega_{c\_upper} = 0.4$ gives the second maximum, and $\omega_{c\_upper} = 0.5$ gives the minimum. Although the density profiles ρ for $\omega_{c\_upper} = 0.3$ and 0.5 are not shown in the figure, we have confirmed that the density profiles of ρ for three values of ω_{c_upper} are about the same by our calculation. Therefore the tendency of ρ_{coke} with respect to the value of ω_{c_upper} is similar to that of $\rho + \rho_{coke}$. Then the density of ρ_{coke} is seen to be larger for a smaller value of ω_{c_upper} in the char zone. This tendency of the relation between ρ_{coke} and ω_{c_upper} conforms to the description of the mathematical model for coking in Subsection 2.2. As stated above, in the region between the surface and $y \approx 3.5$ mm, $\rho + \rho_{coke}$ decreases as y approaches the surface. The reason for this tendency is the same as that discussed in 4.1.2 with respect to Fig. 9. The density profile without coking and ρ for $\omega_{c\_upper} = 0.4$ have approximately the same values for y larger than the value for surface, and increase monotonously as y increases from the surface. When y is larger than about 7 mm, ρ_{coke} is small and the density profile (ρ or $\rho + \rho_{coke}$) for each case is approximately the same.

Figure 14 shows the density distributions with respect to the y axis for $q_{cw} = 0.8$ MW/m^2. The similar results are obtained in this figure except that $\rho + \rho_{coke}$ for each ω_{c_upper} decreases monotonously as y increases from the surface in the
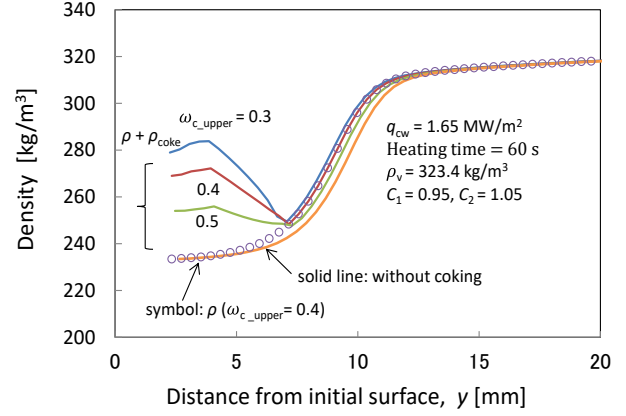

Fig. 13. Effect of ω_{c_upper} upon the density distribution of ablator ($q_{cw} = 1.65$ MW/m^2).
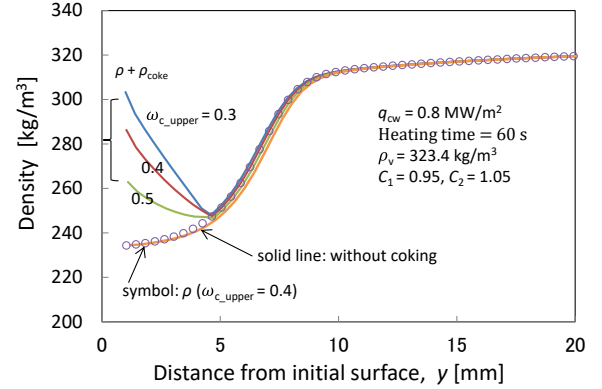

Fig. 14. Effect of ω_{c_upper} upon the density distribution of ablator ($q_{cw} = 0.8$ MW/m^2).

neighborhood of the surface. The reason for this tendency is that this region was not exposed to the temperature higher than 2000 K during the heating because of the low value of $q_{cw} = 0.8$ MW/m^2, from which the coking is not depressed in this region.

5. Conclusions

The coking phenomenon within a lightweight carbon-phenolic ablator exposed to the aerodynamic heating environment of air was investigated analytically and experimentally. The existing one-dimensional transient charring ablation analysis code was modified so that the coking behavior of the ablator can be calculated. Arc-heated tests of the ablators were conducted, where measured density profiles of the ablators were compared with those of calculation. Effects of heating rates and carbon mass fraction in the pyrolysis gas upon the density profile were also examined. The effect of coking upon the surface recession is studied. Main conclusions within the range of this research are as follows:

(1) Basic equations for coking behavior (mass conservation equation of a pyrolysis gas and carbon, and energy equation) are described.

(2) The tendency of the density profile in the region near the surface obtained by measurement is that as x (or y) increases from the point near the surface, the density decreases, reaches

a minimal value, and increases. This tendency is similar to that for the Apollo ablator [13] and a low density LATS ablator in a N_2 environment. [12]

(3) The measured density profiles of the LATS ablators agree well with those by calculation for $\omega_{c\_upper} = 0.3$. The measured density distribution in the low density LATS ablator heated in a N_2 environment in other literature agrees well with that of calculation by our coking calculation code with $\omega_{c\_upper} = 0.4$. These results would support the validity of the mathematical model for coking in the ablation analysis code.

(4) Among the values of $\omega_{c\_upper} = 0.3$, 0.4 and 0.5, which determine the temperature dependency of carbon mass fraction in a pyrolysis gas, the smaller value of ω_{c_upper} gives the higher densities of ρ_{coke} and $\rho + \rho_{coke}$ in the coking region. The density with coking is higher than that without coking in the coking region.

(5) For the three values of ω_{c_upper}, coking is confined mainly within a char zone. Out of this region deep from the surface, ρ_{coke} is small and the density (ρ or $\rho + \rho_{coke}$) for each case is about the same.

(6) The density distributions of ρ for $\omega_{c\_upper} = 0.3$, 0.4 and 0.5 and the density distribution for no coking are about the same.

(7) For the low heating rate (0.8 MW/m^2), as y increases, the density decreases, and after reaching the minimum point it increases. For the high heating rate (1.65 or 1.85 MW/m^2), the tendency of the density is the same as that for the low heating rate except that the region with a rather flat density (or the region in which the density slightly increases as y increases) exists near the surface. The validity of this behavior obtained by the mathematical model for coking in this paper should be examined experimentally in the future.

(8) A higher value of ρ_v gives a lower surface recession ΔS. A smaller value of ω_{c_upper} promotes coking; the surface density increases, which reduces ΔS. Calculated ΔS for "without coking" is the largest. Whereas the number of samples is small, the measured values of ΔS are found to be lower than the calculated ones.

In this paper we have shown that the measured density profiles of a small number of ablator samples agree fairly well with those by calculation using our coking code. However the amount of data is not enough. In order to improve the reliability of calculation by our coking analysis code, more experimental and analytical coking data should be accumulated in the future.

Acknowledgements

References

1) Strauss, E. L.: Superlight Ablative Systems for Mars Lander Thermal Protection, *J. Spacecraft Rockets*, **4** (1967), pp.1304-1309.

2) Sutton, K.: An Experimental Study of a Carbon-Phenolic Ablation Material, NASA TN D-5930, Sept. 1970.

3) Peterson, D. L. and Nicoleit, W. E.: Heat Shielding for Venus Entry Probes, *J. Spacecraft Rockets*, **4** (1974), pp. 382-387.

4) Tran, H., Johnson, C., Rasky, D., Hui, F., Chan, Y. K., and Hsu, M.: Phenolic Impregnated Carbon Ablators (PICA) for Discovery Class Missions, AIAA-96-1911, 1996.

5) Milos, F. S., Chen, Y.-K. and Squire T. H.: Analysis of Galileo Probe Heat Shield Ablation and Temperature Data: Ablation and Thermal Response Program for Spacecraft Heatshield Analysis, *J. Spacecraft Rockets*, **36** (1999), pp. 298-306.

6) Kato, S., Sakata, R., Kanno, Y., Uto, M., Okuyama, K., Uegaki, E., Shingu, S., Ijichi, K. and Inatani, Y.: Development of USERS/REM Heat Shield System and its Evaluation after Re-entry, ISTS2004-e-36, Proceedings of the 24th International Symposium on Space Technology and Science (Selected Papers), Miyazaki, Japan, 2004, pp. 621-628.

7) Kontinos, D. A. and Stackpoole, M.: Post Flight Analysis of the Stardust Sample Return Capsule Earth Entry, AIAA-2008-1197, 2008.

8) Yamada, T., Ishii, N., and Inatani, Y.: Post Flight Analysis of the Hayabusa Sample Return Capsule, 2011-def-03, 28th International Symposium on Space Technology and Science, 5-12 June, Okinawa Prefecture, Japan.

9) Okuyama, K., Kato, S., and Ohya, H.: Thermochemical Performance of a Lightweight Charring Carbon Fiber Reinforced Plastic, *Trans. Jpn. Soc. Aeronaut. Space Sci.*, **56** (2013), pp.159-169.

10) Kato, S., Okuyama, K., Gibo, K., Miyagi, T., Suzuki, T., Fijita, K., Sakai, T., Nishio, S., and Watanabe, A.: Thermal Response Simulation of Ultra Light Weight Phenolic Carbon Ablator by the Use of the Ablation Analysis Code, *Trans. JSASS Aerospace Technology Japan*, **10**, ists28 (2012), pp. Pe_31- Pe_39.

11) Kondo, J.: *High Speed Aerodynamics*, 1977, pp.541-546, Corona (in Japanese).

12) Sakai, T., Okuyama, K., Kobayashi, Y., Tomita, M., Suzuki, T., Fujita, K., Kato, S., and Nishio, S.: Post Test Sample Analysis of a Low Density Ablator Using Arcjet, *Trans. JSASS Aerospace Technology Japan*, **10**, ists28 (2012), pp. Pe_65- Pe_71.

13) Bartlett, E. P., Abbett, M. J., Nicolet, W. E., and Moyer, C. B.: Improved Heat-Shield Design Procedures for Manned Entry Systems, Part 2, Application to Apollo, Aerotherm Final Report, No. 70-15, 1970.

14) Moyer, C. B. and Rinadal, R. A.: An Analysis of Coupled Chemically Reacting Boundary Layer and Charring Ablator, Part II, Finite Difference Solution for the In-Depth Response of Charring Materials Considering Surface Chemical and Energy Balances, NASA CR-1061, 1967.

15) Potts, R. L.: Application of Integral Methods to Ablation Charring Erosion, A Review, *J. Spacecraft Rockets*, **32** (1995), pp. 200-209.

16) Potts, R. L.: Hybrid Integral/Quasi-Steady Solution of Charring Ablation, AIAA-90-1677, 1990.

17) Suzuki, T., Fujita, K., Sakai, T., Okuyama, K., Kato, S., and Nishio, S.: Thermal Response Analysis of Low Density CFRP Ablator, *Trans. JSASS Aerospace Technology Japan*, **10**, ists28 (2012), pp. Pe_21-Pe_30.

18) Chen, Y.-K. and Milos, F. S.: Ablation and Thermal Response Program for Spacecraft Heatshield Analysis, *J. Spacecraft Rockets,* **36** (1999), pp. 475-483.

19) Kato, S., Okuyama, K., Nisio, S., Sakata, R., Hama, K., and Inatani, Y.: Numerical Analysis of Charring Ablation for Ablative Materials of Re-Entry Capsules, *J. Jpn. Soc. Aeronaut. Space Sci.,* **50** (2002), pp. 255-263 (in Japanese).

20) Ladacki M., Hamilton J. V., and Cohz S. N.: Heat of Pyrolysis of Resin in Silica-Phenolic Ablator, *AIAA J.*, **4** (1965), pp. 1798-1802.

21) Swan, R. T., Approximate Analysis of the Performance of Char Forming Ablators, NASA TR-R195, 1964.